metals

MDPI

Article

Effects of Ultrasonic Vibration on the Transport Coefficients in Plasma Arc Welding

Yongfeng Li, Chuansong Wu * and Maoai Chen

MOE Key Lab for Liquid-Solid Structure Evolution and Materials Processing, Institute of Materials Joining, Shandong University, Jinan 250061, China; lyf452433605@126.com (Y.L.); chenmaoai@sdu.edu.cn (M.C.)
* Correspondence: wucs@sdu.edu.cn; Tel.: +86-531-8839-2711

Received: 11 February 2020; Accepted: 25 February 2020; Published: 27 February 2020



Abstract: In ultrasound assisted plasma arc welding (U-PAW), the exerted ultrasonic vibration on the tungsten electrode interacts with the plasma arc and changes its heat-pressure characteristics. It is of great significance to investigate the underlying interaction mechanism. In this study, the calculation method of transport coefficients in U-PAW is developed. Translational thermal conductivity (including electrons thermal conductivity and the thermal conductivity of heavy particles) and electrical conductivity are calculated by considering the second-order approximation of Maxwell velocity distribution function, while the method of Butler et al. is adopted to calculate the reaction thermal conductivity in U-PAW. The effective value of the ultrasound velocity gradient tensor is employed to describe the effects of ultrasonic vibration on transport coefficients in ultrasound assisted plasma arc. The calculation results show that when the ultrasound is applied, the thermal conductivity of heavy particles in the plasma increases significantly and the electron thermal conductivity increases within some extent. The thermal conductivity of the reaction also increased to a great extent, and the electrical conductivity decreases a little bit. Although the thermal diffusion coefficient also has some increase, but the ordinary diffusion coefficient is obviously reduced due to the application of the ultrasound. With the updated transport coefficients, the plasma arc pressure on the anode surface is numerically computed, and the predicted pressures of PAW and U-PAW can be consistent with the measured ones.

Keywords: ultrasound; plasma arc; transport coefficients; plasma arc pressure

1. Introduction

Plasma arc welding (PAW) has the advantages of large arc column stiffness, high heat intensity, large weld depth-to-width ratio, narrow heat affected zone [1], etc. In PAW, a keyhole penetrating through the workpiece can be formed in the molten pool, which makes both the heat and pressure of plasma arc act along the plate thickness so that large penetration depth and depth-to-width ratio welds are obtained. Compared with other high-energy beam (laser and electron beam) welding processes, PAW process is low in equipment cost, convenient in maintenance and operation, and strong in adaptability [2], so it has great application potential in manufacturing structures with medium thickness. However, conventional PAW still has some shortcomings, such as an insufficient keyholing ability and poor stability of the keyhole and weld pool [3]. Recently, investigators have modified the conventional PAW to overcome the aforementioned problems. Radial gas at the torch exit [4], the hybrid weld process [5–7], and controlled pulse with a specially designed current waveform [8,9] have been tried. However, all these methods increase the complexity of the process and equipment, which causes an inconvenience to practical operation and application.

As a type of mechanical energy, ultrasound is widely used in the field of material processing [10,11]. Wu et al. [12] applied ultrasonic vibration to the tungsten electrode in PAW torch, and then acoustic

energy field is exerted in the plasma arc. The interaction between the ultrasonic vibration and the plasma arc affects the heat intensity and pressure of the plasma arc so that its keyholing capability is improved. Although the interaction mechanism of ultrasound and plasma arc was analyzed from a macro perspective point of view [13], it is the effect of ultrasonic vibration on the microscale motion of the particles inside the plasma, which plays a critical role in determining the macroscale variation of both the heat intensity and pressure of the plasma arc.

The Maxwell velocity distribution function of the particles in gas connects the macroscopic properties of gas with the microscopic collisions of particles. The transport properties of gas can be expressed by the velocity distribution function. Therefore, if we know the influence law of ultrasound on the velocity distribution function of gas, we can analyze the influence of ultrasound on the gas transport coefficients through theoretical analysis and numerical calculation. The general theory and calculation method of gas transport coefficients have been systematically studied [14–16], and many researchers have also calculated the transport coefficients of various gases such as argon and helium, including the calculation of transport coefficients of two-temperature plasma [17,18] and mixed plasma [19,20]. The roles of shielding gas and metal vapour in affecting the plasma arc [21–24] and the coupling mechanism of plasma arc-keyhole-weld pool [25–27] have been numerically simulated. The energy balance and transport coefficients have a significant impact on arc pressure [28]. The thermodynamics study of plasma arc is the basis for studying heat transfer and flow in molten pool [29,30]. However, to our best knowledge, no one has studied how the exerted ultrasound affects the plasma transport coefficients until now.

In this study, the influence mechanisms of ultrasound on plasma transport coefficients (thermal conductivity, electrical conductivity, and diffusion coefficient) are taken into consideration, and the transport coefficients in the ultrasound interacted plasma arc are calculated. Such transport coefficients are applied in modeling the ultrasound assisted plasma arc welding (U-PAW), and numerical simulation is conducted to analyze the effects of ultrasound on the arc pressure.

2. Modelling of U-PAW Process

When ultrasound propagates in gas, it causes the change of particles motion state in gas, and the gas transport coefficients (thermal conductivity, diffusion coefficient and electrical conductivity, etc.) are closely related to the collision of particles in gas. Applying ultrasound to the plasma arc will not only produce sound pressure that fluctuates with time macroscopically [13], but also affects the thermal conductivity, diffusion coefficient, and electrical conductivity of plasma. Therefore, it is necessary to study the underlying mechanism how the ultrasound inducing variation of transport coefficients affects the physical characteristics of plasma arc. To this end, a model is developed to describe the ultrasound assisted plasma arc. Figure 1 shows the calculation domain, including the tungsten electrode, nozzle, plasma arc area, and the anode.

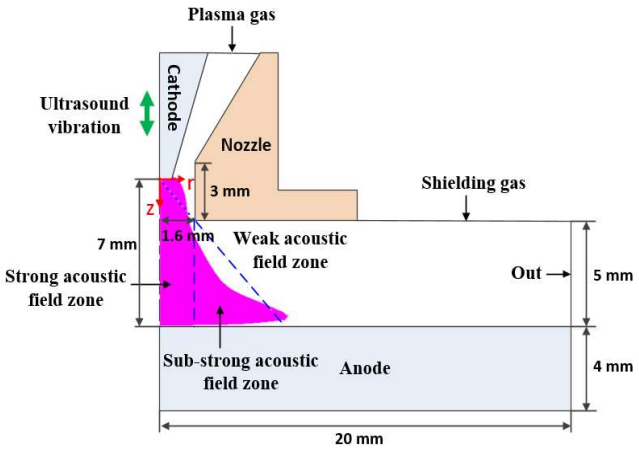

Figure 1. Schematic illustration of numerical model for U-PAW (ultrasound assisted plasma arc welding).

2.1. Ultrasound Propagation in Plasma Arc

Ultrasound propagation in plasma arc is different from that in static gas at normal temperature and pressure, because plasma jet is with high temperature and high flow velocity. When other conditions remain unchanged, the higher the temperature of the plasma, the faster the ultrasonic propagation speed [31]. Because only longitudinal wave exists in a fluid medium, transverse wave generated by tungsten electrode is not considered here. As the propagation speed of ultrasound wave is closely related to the temperature of the plasma arc, the higher the temperature, the faster the propagation speed of the ultrasonic wave. As demonstrated in Figure 1, the plasma arc column with higher temperature is taken as a strong acoustic field region, the periphery of plasma arc is considered as a sub-strong acoustic field region, and the region outside plasma arc with low temperature is defined as a weak acoustic field region. In fluid media, sound pressure is generally used as the characteristic quantity of the acoustic field, and the equation of the acoustic field can be expressed as [32]:

$$\frac{\partial^2 p_s}{\partial r^2} + \frac{\partial^2 p_s}{\partial z^2} = \frac{1}{c^2}\frac{\partial^2 p_s}{\partial t^2} \tag{1}$$

$$c = c_{ref}\sqrt{\frac{T}{T_{ref}}} \tag{2}$$

where p_s is acoustic pressure, t is time, c is propagation velocity of ultrasound in plasma arc, c_{ref} is propagation velocity of ultrasound under normal temperature and pressure, and T_{ref} is thermodynamic reference temperature (273.15 K). The distribution of ultrasound in plasma arc can be obtained by solving the above equation. The sound pressure amplitude is expressed by [31]:

$$p_{ms} = \rho c u_m \tag{3}$$

$$u_m = \omega \cdot A_v = 2\pi f_v \cdot A_v \tag{4}$$

where p_{ms} is acoustic pressure amplitude, ρ is mass density, u_m is velocity amplitude of ultrasonic vibration, ω is angular frequency of ultrasonic vibration, f_v is frequency of ultrasonic vibration, A_v is amplitude of ultrasound. Since only the ultrasound propagation is calculated in plasma arc in this study, the surface of workpiece and outer boundary (including outlet, shielding gas inlet, nozzle and plasma gas inlet) are all set to a given sound pressure flux [33]:

$$\frac{\partial p_s}{\partial \vec{n}} = \gamma_s\left(p_s - p_{ref}\right) \tag{5}$$

where γ_s is the acoustic pressure flux of boundary, p_{ref} is reference acoustic pressure in gas. The ultrasound is a simple harmonic wave satisfying the rule of sinusoidal vibration, and the sound pressure at the tip of the tungsten electrode is written as:

$$p_s = p_{ms} \cdot \sin(\omega\, t) \tag{6}$$

where the acoustic pressure amplitude p_{ms} is dependent on the overall temperature of the plasma arc, the corresponding gas density, and ultrasound propagation speed.

2.2. Numerical Model of U-PAW

We have developed a numerical model of the ultrasound assisted plasma arc [13], which is used to analyze the variation of arc pressure on the workpiece surface when ultrasound propagates in the plasma arc. It is found that ultrasound increases the peak value of plasma arc pressure. However, the treatment of ultrasound in plasma arc was simplified in [13], i.e., a source term of sound pressure was

added to the momentum equation. The influence of ultrasound on the thermal conductivity (k) and electrical conductivity (σ) used in the governing equations was not considered.

In this study, the influence of ultrasonic vibration on the transport coefficients is analyzed, and the varied transport coefficients in ultrasound assisted plasma arc are calculated. Then, the modified transport coefficients are used to calculate the plasma arc pressure under action of ultrasound. The details of the U-PAW model including the governing equations and boundary conditions can be referred to [13], which are not reiterated here. Next, we focus on how to determine the thermal conductivity and electrical conductivity of the plasma arc when ultrasonic vibration is exerted on it.

3. Transport Coefficients in Ultrasound Assisted Plasma Arc

Viscosity, heat conduction, and diffusion in non-uniform gas represent the trends of macro velocity, so temperature and composition of the gas towards to homogenization According to the theory of molecular motion, the homogenization trends are caused by the movement of molecules from one point to another. This movement tends to homogenize the states at both ends of each mean free path by transporting the average momentum and average energy at the starting point to the other end [15]. Generally speaking, the velocity distribution function at each point in a gas always changes rapidly by the collision of molecules, but in fact, the state at a certain point is only significantly affected by the particles directly adjacent to it, i.e., within the distance of several mean free paths. This means that a molecule can seldom directly transfer its energy and momentum to molecules beyond the distance of several mean free paths, and energy and momentum transport must be made through the "relay" among adjacent molecules. This causes the energy and momentum differences among most of the colliding molecules to be within a certain range.

For argon plasma, we first estimate its mean free path. Electrons and heavy particles are regarded as two different particles. The mean free paths of heavy particles and electrons are calculated according to the following equations [15]:

$$l_h = \frac{\sqrt{2}}{2\pi n_h \sigma_h^2} \tag{7}$$

$$l_e = \frac{1}{\pi} \cdot \left[\sqrt{2} \cdot n_e \sigma_e^2 + n_h \left(\frac{\sigma_e + \sigma_h}{2} \right)^2 \cdot \left(1 + \frac{m_e}{m_h} \right)^{1/2} \right]^{-1} \tag{8}$$

where l is the mean free path, σ is the diameter, m is the mass, and n is the number density of particles. The subscripts h and e represent heavy particles and electrons, respectively. Here, n_h includes argon atom number density n_0, Ar^+ number density n_1 and Ar^{2+} number density n_2. Under the condition of local thermodynamic equilibrium, the composition of plasma can be calculated by the Saha equation combined with Dalton's law and electric neutral condition [34–36].

Saha equation:

$$\frac{n_e n_i}{n_{i-1}} = \frac{Q_e Q_i}{Q_{i-1}} \left(\frac{2\pi m_e k_b T}{h_p^2} \right)^{\frac{3}{2}} \exp\left(-\frac{\varepsilon_i - \Delta\varepsilon_i}{k_b T} \right) \tag{9}$$

where subscript $i = 1, 2$ means Ar^+ and Ar^{2+}, Q_i is the partition function of particle i, Q_e is the statistical weight of electron $Q_e = 2$, T is temperature, h_p is Planck constant, k_b is Boltzmann constant, ε_i is the ionization energy of the i-times ionized atom, and $\Delta\varepsilon_i$ is the decrease of ionization energy which is calculated by [37]:

$$\Delta\varepsilon_i = \frac{Ze^2}{4\pi\varepsilon_0 \lambda_D} \tag{10}$$

$$\lambda_D = \left[\frac{\varepsilon_0 k_b T}{e^2 n_e} \right]^{1/2} \tag{11}$$

where ε_0 is the vacuum dielectric constant, e is the electron charge, λ_D is the Debye length, and Z is the number of charges carried by ions.

Dalton's law:

$$p = (n_0 + n_1 + n_2 + n_e)k_bT \tag{12}$$

where p is the pressure.

Charge quasi-neutrality condition:

$$n_e = \sum_{Z=1}^{2} Z \cdot n_Z \tag{13}$$

The argon plasma calculated here contains four kinds of particles, Ar, Ar^+, Ar^{2+}, and e. The changes of various particle densities with temperature are shown in Figure 2.

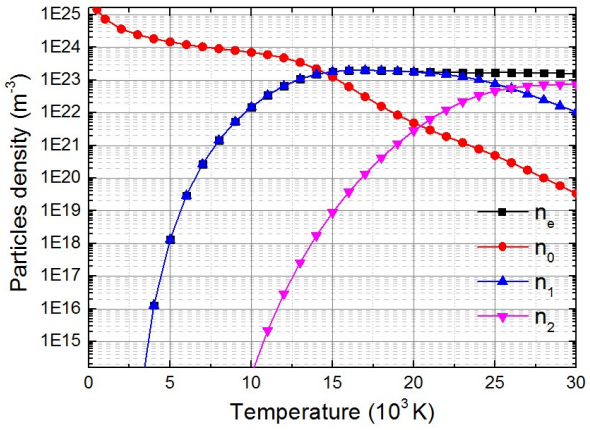

Figure 2. Number density of different particles in plasma versus temperature.

When the temperatures are 4×10^3 K and 2×10^4 K, the mean free paths of heavy particles are 9.463×10^{-7} m and 9.406×10^{-6} m, respectively. Since the ultrasonic vibration amplitude applied to the plasma arc is 2×10^{-5} m, the mean free path of heavy particles is always less than the vibration amplitude of ultrasound. Thereby, under the action of ultrasonic vibration, heavy particles can be driven to move beyond their mean free path distance, and can interact with particles with larger energy and momentum than themselves. Taking the heavy particle 'A' in Figure 3 as an example, the macro velocity of the fluid is not considered temporally. Due to the ultrasound action, 'A' will vibrate to different positions where the particles have different energies. When 'A' reaches the position 'a' where the energy of the surrounding particles is higher, 'A' will also become the particle with a similar energy because of collision among particles. When 'A' vibrates downward to reach the position 'b' where the temperature is lower relative to the position 'a', the energy of 'A' will become close to the particles at the position 'b' because of collision among particles. For the whole process, it can be seen that 'A' brings part of the energy from the position 'a' to the position 'b'. This process is repeated so as to promote the heat transfer and increase the thermal conductivity.

For electrons, the mean free paths are 5.352×10^{-6} m at 4×10^3 K and 5.32×10^{-5} m at 2×10^4 K, respectively. At low temperature, the mean free path of electrons is less than the ultrasonic vibration amplitude. With the increase of temperature, the mean free path of electrons gradually exceeds the vibration amplitude. Although ultrasound cannot directly cause the reciprocating vibration of electrons, it can cause such vibration of heavy particles including Ar^+ and Ar^{2+}. According to Debye shielding theory [15], charged particles tend to attract opposite charges with slightly more than their own amount of charge to their vicinity, forming shielding effect around it. When the charged heavy particles vibrate under the action of ultrasound, they will attract the electrons nearby to move with them, resulting the effect of ultrasound on the electron motion.

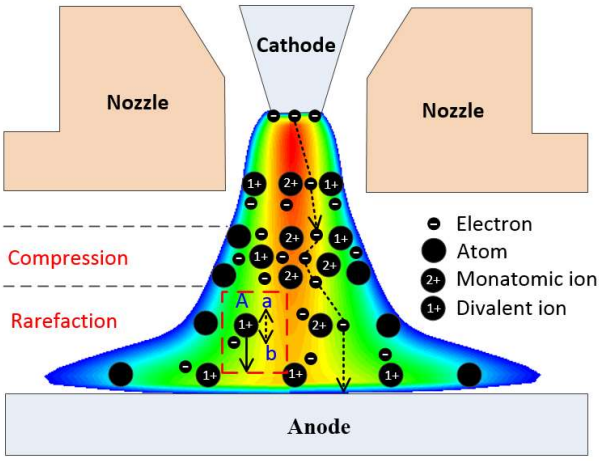

Figure 3. Schematic of particles motion in plasma arc with ultrasonic effect.

In addition, the electrons emitted from the tip of the tungsten electrode make the plasma arc electrically conductive, but the emitted electrons cannot reach the anode surface directly, and instead rely on ionized argon gas in the plasma arc as a conductive medium. Electrons will be affected by various particles in the diffusion process. Without ultrasound, the density of various particles fluctuates very little, thus having little influence on the diffusion velocity of electrons. The application of ultrasound affects the movement of electrons and causes the density of electrons to change, but it does not mean that ultrasound promotes the movement of electrons between the tungsten electrode and the anode. On the contrary, due to the density change of heavy particles (especially charged heavy particles) and electrons, the high density region will form a "particle wall" that moves directionally at a certain speed, hindering the diffusion movement of electrons, causing the mean free path of electrons in the "particle wall" to decrease and the collision frequency to increase. Therefore, the ultrasound improves the thermal conductivity of electrons and reduces the ordinary diffusion coefficient of electrons which is closely related to electrical conductivity, thus decreasing the electrical conductivity of plasma arc. In addition, ultrasound will influence the thermal conductivity of the reaction. Some Ar atoms and Ar^+ will absorb heat and ionize at the same time in the high-temperature region. When these particles are brought to the low-temperature region by ultrasound, the decrease in temperature will lead to the recombination of Ar^{2+} and Ar^+ with electrons and release energy. Subsequently, the particles will return to the high-temperature region and ionize again under the effect of ultrasound, thus the heat transfer will be promoted repeatedly.

3.1. Normal Plasma Arc

Researchers have studied the transport coefficients in normal plasma [38–41] based on following assumptions: (1) Only the elastic collision process among particles is considered, i.e., and the effect of collision on the internal energy of particles is ignored. (2) Compared to dense gas (gas pressure > 1 MPa), the studied gas or plasma is thin enough, so that only two-body collisions between particles need to be considered. It is required that the duration of one collision between particles is much less than the interval between two collisions. (3) Since the mass ratio of heavy particles and electrons is very large, the speed of energy exchange between them is very low. It is assumed that the energy exchange between heavy particles and electrons can be neglected relative to the energy exchange between heavy particles as well as electrons and electrons [14].

The gas transport coefficient is in essence the macroscopic description of the collisions among microscopic particles. The tool to describe the statistical law of microscopic particles is the velocity distribution function f. To determine the thermal conductivity, diffusion coefficient, and electrical conductivity, we need to know the corresponding physical quantities (heat flux vector $\vec{q}$, diffusion velocity $\vec{C}_j$ and conduction current density $\vec{j}_e$) firstly, and then establish the relationship between

these physical quantities and the velocity distribution function f. To conduct such calculation for normal plasma arc, only the first order approximation of the velocity distribution function ($f^{(0)} + f^{(1)}$) is used [15]. The transport quantity can be described as follows:

$$\text{Transport flux} = (\text{Transport coefficient}) \times (\text{Driving force})$$

Thereby, if the heat flux vector $\vec{q}$, diffusion velocity $\overrightarrow{C}_j$ and conduction current density $\vec{j}_e$ are known, we can obtain the formulas of thermal conductivity, diffusion coefficient and conductivity. Through the transformation of the formula, the formula of transport coefficient can be expressed by bracket integrals $q_{ij}^{m_0 p_0}$. The bracket integrals can be expressed in the form of collision integrals, so in the end we can get the value of the transport coefficients by finding the corresponding collision integrals. The details of such calculation may be referred to [14,38,40].

3.2. Ultrasound Assisted Plasma Arc

When ultrasound is applied to plasma gas, the velocity distribution function must be expressed by the second-order approximation ($f^{(0)} + f^{(1)} + f^{(2)}$). An additional assumption has to be made, i.e., the gas under ultrasound action will quickly reach the equilibrium state because the period of ultrasonic vibration is much longer than the relaxation time.

3.2.1. (1) Thermal Conductivity Variation of Heavy Particles and Electrons Caused by Ultrasound

Thermal conductivity can be divided into translational, reactive and internal components. The translational and reactive components of thermal conductivity variation caused by ultrasound are calculated in this and next subsections, respectively. According to references [42,43], the ratio of internal thermal conductivity to thermal conductivity is very small, so it is not considered in this paper.

When ultrasound is applied, the heat flux of the gas becomes following form,

$$\begin{aligned}\vec{q} = {} & \tfrac{5}{2}k_b T\sum_j\left(1-\tfrac{2}{5}\tfrac{\rho}{n}\sum_i \frac{(E_{ij})_{us}(D_i^T)_{us}}{n_i m_i}\right)n_j\overrightarrow{C}_j \\ & -\left[-\frac{5k_b}{4}\sum_j n_j\left(\frac{2k_bT}{m_j}\right)^{\frac{1}{2}}a_{j1}+\frac{\rho k_b}{n}\sum_{i,j}\frac{(E_{ij})_{us}(D_i^T)_{us}\left(D_j^T\right)_{us}}{n_i m_i m_j}\right]\nabla T \\ & +\sum_j\left(\frac{125}{8}-\frac{7}{4}\frac{T}{\mu_j}\frac{d\mu_j}{dT}\right)\cdot\frac{\mu_j^2}{\rho_j T}\cdot\nabla\cdot\vec{c}_0\cdot\nabla T\end{aligned} \tag{14}$$

where n is the total number density of all particles, $\overrightarrow{C}_j$ is diffusion velocity [16,44], a_{j1} is the Sonine expansion coefficient [45] (its subscripts are defined at the end of this paragraph), $\left(E_{ij}\right)_{us}$ is an element of an inverse matrix of a matrix whose element is $\left(D_{ij}\right)_{us}m_j$, while $\left(D_{ij}\right)_{us}$ is an ordinary diffusion coefficient when ultrasound is applied, and $\left(D_i^T\right)_{us}$ is a thermal diffusion coefficient when ultrasound is applied, μ_j is viscosity, $\vec{c}_0$ is vibration velocity of particles, and $\nabla\cdot\vec{c}_0$ will be explained in paragraph (5) of the subsection. For the Sonine expansion coefficient a_{j1}, its first subscript j may represent electrons or other particles, and its second subscript 1 represents the 1st Sonine polynomial expansion coefficient [16].

At the right-hand side of the Equation (14), the first, second and third terms represent the flux of energy due to mass transport, temperature gradient and ultrasonic vibration, respectively. Thereby, a general equation for the thermal conductivity of plasma when ultrasound is applied is obtained:

$$\begin{aligned}\lambda_{us} = {} & -\frac{5k_b}{4}\sum_j n_j\left(\frac{2k_bT}{m_j}\right)^{\frac{1}{2}}a_{j1}+\frac{\rho k_b}{n}\sum_{i,j}\frac{(E_{ij})_{us}(D_i^T)_{us}\left(D_j^T\right)_{us}}{n_i m_i m_j} \\ & +\sum_j\left(\frac{125}{8}-\frac{7}{4}\frac{T}{\mu_j}\frac{d\mu_j}{dT}\right)\cdot\frac{\mu_j^2}{\rho_j T}\cdot\nabla\cdot\vec{c}_0\end{aligned} \tag{15}$$

Equation (15) is a general formula for plasma thermal conductivity when ultrasound is applied. Since the plasma contains heavy particles and electrons, the difference in diffusion coefficient and viscosity results in the difference in electron thermal conductivity and heavy particle thermal conductivity. For heavy particles, the second term in Equation (15) can be ignored relative to the first term [46], so the thermal conductivity formula of heavy particles when ultrasound is applied is as follows:

$$\lambda_{h-us} = \theta_T \cdot \theta_M \cdot \sum_j \left(\frac{125}{8} - \frac{7}{4} \frac{T}{\mu_j} \frac{d\mu_j}{dT} \right) \cdot \frac{\mu_j^2}{\rho_j T} \cdot \nabla \cdot \vec{c}_0 - \frac{5k_b}{4} \sum_j n_j \left(\frac{2k_b T}{m_j} \right)^{1/2} a_{j1} \tag{16}$$

In Equation (16) the first term on the right-hand side is the additional thermal conductivity due to the application of ultrasound, and the second term is the thermal conductivity of heavy particles when no ultrasound is applied. Further,θ_T represents the correction coefficient related to temperature. Because the second-order approximate formula of diffusion velocity is derived under the conditions of low temperature, gas density 10^{-5} times of normal density, or shock wave, and here we use it to high-temperature plasma arc, the equation needs to be corrected. It is known that sound propagation velocity and temperature have the relationship [31]:

$$c = c_{ref} \left(\frac{T}{T_{ref}} \right)^{1/2} \tag{17}$$

We get the correction coefficient:

$$\theta_{\mathrm{T}} = \left(\frac{T}{T_{ref}} \right)^{1/2} \tag{18}$$

Since the diffusion coefficient of heavy particles is small, the second term in Equation (15) can be ignored in calculating the thermal conductivity of heavy particles. Because normal gas density is used, we introduce a corrected coefficient by considering the factors of temperature and gas density.

$$\theta_M = a_1 + a_2 \cdot \log \left(\frac{n_h}{n_{ref}} \right) \tag{19}$$

where θ_M is the correction coefficient related to the concentration of heavy particles, a_1 and a_2 refer to the actual measured values of a series of arc pressures to obtain a series of θ_M values under different welding parameters, and then a_1 and a_2 are obtained through linear fitting.

According to reference [45], when calculating the electronic thermal conductivity, the first term on the right side of equation (15) actually includes terms related to electrons ($j = 1$) and heavy particles ($j \neq 1$), but the term corresponding to $j = 1$ is very large in the ionized gas, while the other terms are less than 1% and can be ignored. In addition, the viscosity of electron is very small. So, the thermal conductivity formula of electron when ultrasound is applied as follows:

$$\lambda_{e-us} = -\frac{5k_b}{4} n_e \left(\frac{2k_b T}{m_e} \right)^{1/2} a_{11} - \frac{\rho k_b}{n} \frac{\left(D_e^T \right)_{us}^2}{n_e m_e^3 (D_{ee})_{us}} \tag{20}$$

where the first term is not affected by ultrasound, which is the same as that in Equation (15). Although the second term in Equation (20) also exists when ultrasound is not applied, the diffusion coefficient in the second term can be affected when ultrasound is applied, thus causing the change of electron thermal conductivity. The last term of Equation (15) is related with the viscosity of electrons. Since the viscosity of electrons is very small, the last term can be ignored for calculating electron thermal conductivity.

3.2.2. (2) Reaction Thermal Conductivity Variation Caused by Ultrasound

In reference [43] the formula for calculating the reaction thermal conductivity of conventional plasma was given. Here the effect of ultrasound on the reaction thermal conductivity must be considered, so we need to deduce a new formula for reaction thermal conductivity.

The ionization of argon atoms is closely related to temperature, and the ionization rate of argon plasma is different at different temperatures. When ultrasound propagates in argon plasma, it will drive the particles in the plasma to move back and forth, which will also cause the same particle's position to change periodically. Because the temperatures in different positions in the plasma arc are different, we assume that there is a very small volume, and the particles in the cube will move back and forth under the drive of ultrasound. When the volume is at a higher temperature position, the ionization rate will increase, thus absorbing some energy. When the cube is at a lower temperature position, the ionization rate will decrease, while the particle recombination will release some energy, thus realizing energy transport. According to the above theory, we can deduce as follows:

$$\vec{q}_{r-us} = -\lambda_{r-us}\nabla T \tag{21}$$

where λ_{r-us} is reaction thermal conductivity caused by ultrasonic vibration. According to the definition of heat flux, $\vec{q}_{r-us}$ can be expressed as a function of ultrasonic amplitude and argon plasma ionization rate. We take a very small cross section with an area of S to study. Under the effect of ultrasonic vibration, the maximum distance that the section can move is $2A_v$, and its effective value $\sqrt{2}A_v$, The temperature difference between the two ends of the distance can be expressed as $\sqrt{2}A_v\nabla T$, and the number of particles in the volume is $n_h\sqrt{2}A_vS$. The ionization rate difference per unit temperature in this region is $\frac{I_{T_1}^{(1)}-I_{T_2}^{(1)}}{T_1-T_2}$ and $\frac{I_{T_1}^{(2)}-I_{T_2}^{(2)}}{T_1-T_2}$, T_1 and T_2 are the temperatures at both ends of the distance, respectively, and $I_{T_1}^{(1)}$, $I_{T_2}^{(1)}$, $I_{T_1}^{(2)}$ and $I_{T_2}^{(2)}$ represent the primary ionization rate and secondary ionization rate at T_1 and T_2. So

$$\vec{q}_{r-us} = -\frac{2\frac{I_{T_1}^{(1)}-I_{T_2}^{(1)}}{T_1-T_2}\cdot\nabla T\cdot n_h\cdot {A_v}^2\varepsilon_1}{T_{us}} - \frac{2\frac{I_{T_1}^{(2)}-I_{T_2}^{(2)}}{T_1-T_2}\cdot\nabla T\cdot n_h\cdot {A_v}^2\varepsilon_2}{T_{us}} \tag{22}$$

where the first term on the right side of the formula is the heat flux generated by the primary ionization and recombination of argon plasma during ultrasonic vibration, and the second term is the heat flux generated by the secondary ionization and recombination of argon plasma during ultrasonic vibration. Substituting Equation (22) into (21) can obtain

$$\lambda_{r-us} = \frac{2\frac{I_{T_1}^{(1)}-I_{T_2}^{(1)}}{T_1-T_2}\cdot n_h\cdot {A_v}^2\varepsilon_1}{T_{us}} + \frac{2\frac{I_{T_1}^{(2)}-I_{T_2}^{(2)}}{T_1-T_2}\cdot n_h\cdot {A_v}^2\varepsilon_2}{T_{us}} \tag{23}$$

3.2.3. (3) Diffusion Coefficient Variation Caused by Ultrasound

To determine the contribution of the second order approximation of the velocity distribution function to the diffusion velocity, we need to calculate the diffusion velocity of the binary gas, and then we use the relationship between the diffusion coefficient of a multicomponent gas and the diffusion coefficient of the binary gas in [14] to achieve our goals.

For the binary gas, the second-order approximation adds nine new terms to the diffusion velocity $\vec{C}_1 - \vec{C}_2$. After further simplification and transformation [15,47], the diffusion velocity may be written as follows:

$$\begin{aligned}\left(\vec{C}_1 - \vec{C}_2\right)' = {} & \tfrac{2}{3}\tfrac{n^4 m_1 m_2}{p\rho}\tfrac{D'_{12}D^T}{n_1 n_2}\left(\tfrac{3}{2} - \tfrac{T}{D^T}\tfrac{\partial D^T}{\partial T}\right)\cdot\nabla\cdot\vec{c}_0\cdot\tfrac{\partial \ln T}{\partial \vec{r}} \\ & + \tfrac{2}{3}\tfrac{n^4 m_1 m_2}{p\rho}\tfrac{D'^2_{12}}{n_1 n_2}\left(3 - \tfrac{T}{D'_{12}}\tfrac{\partial D'_{12}}{\partial T}\right)\cdot\nabla\cdot\vec{c}_0\cdot\vec{d}_{12}\end{aligned} \tag{24}$$

$$\vec{d}_{12} = \nabla x_1 + \frac{n_1 n_2 (m_2 - m_1)}{n\rho} \Delta \ln p - \frac{\rho_1 \rho_2}{\rho p}\left(\vec{F}_1 - \vec{F}_2\right) \tag{25}$$

where $\vec{C}_1$ and $\vec{C}_2$ are particle specific velocity relative to the plasma of the different particles, respectively. D'_{12} is the ordinary diffusion coefficient of the binary gas, so as to be distinguished from the ordinary diffusion coefficient D_{12} of the multicomponent gas, D^T is the binary thermal diffusion coefficient, $\vec{d}_{12}$ is diffusion driving force [15], including concentration gradient, pressure gradient, and external force, while $\vec{F}_1$ and $\vec{F}_2$ are forces exerted on molecules by the external field.

In Equation (24), the first term on the right-hand side is the diffusion velocity term due to temperature gradient and the divergence of ultrasonic vibration velocity ($\nabla \cdot \vec{c}_0$), and the second term is the diffusion velocity term due to diffusion driving force and ultrasonic velocity gradient. Because the diffusion coefficients in this section are obtained from a binary gas, D'_{12} and D^T in Equation (24) need to be transformed [14]:

$$D'_{12} = \frac{\rho_1}{\rho_2} \frac{(\rho/n)^2}{m_1 m_2} D_{ee} \tag{26}$$

$$D^T = \frac{n_1}{n} \frac{\rho/n}{m_2} D_e^T \tag{27}$$

Substituting Equations (26) and (27) into Equation (24) and conducting some manipulation, we get the variation of the diffusion coefficient of plasma arc with ultrasound,

$$\begin{aligned} \left(D_e^T\right)_{add} &= -\tfrac{2}{3}\tfrac{\rho_e \rho^2 D_{ee}}{\rho_h p}\tfrac{n_e}{n^2 m_h} D_e^T \left(\tfrac{3}{2} - \tfrac{n^2 m_h T}{n_e \rho D_e^T}\tfrac{\partial}{\partial T}\left(\tfrac{n_e \rho D_e^T}{n^2 m_h}\right)\right)\nabla \cdot \vec{c}_0 \\ &\approx -\tfrac{2}{3}\tfrac{\rho_e n_e \cdot (n-n_e) D_{ee}}{p n^2} D_e^T \left(\tfrac{3}{2} - \tfrac{n^2 T}{n_e (n-n_e) D_e^T}\tfrac{\partial}{\partial T}\left(\tfrac{n_e (n-n_e) D_e^T}{n^2}\right)\right)\nabla \cdot \vec{c}_0 \end{aligned} \tag{28}$$

$$\begin{aligned} (D_{ee})_{add} &= -\tfrac{2}{3}\tfrac{\rho_e^2 \rho^3 D_{ee}}{\rho_h^2 p n^2 m_e m_h} \cdot D_{ee}\left(3 - \tfrac{n^2 \rho_h m_e m_h T}{\rho_e \rho^2 D_{ee}}\tfrac{\partial}{\partial T}\left(\tfrac{\rho_e \rho^2}{\rho_h n^2 m_e m_h} D_{ee}\right)\right)\nabla \cdot \vec{c}_0 \\ &\approx -\tfrac{2}{3}\tfrac{\rho_e n_e \cdot (n-n_e) D_{ee}}{p n^2} \cdot D_{ee}\left(3 - \tfrac{n^2 T}{n_e (n-n_e) D_{ee}}\tfrac{\partial}{\partial T}\left(\tfrac{n_e (n-n_e) D_{ee}}{n^2}\right)\right)\nabla \cdot \vec{c}_0 \end{aligned} \tag{29}$$

where D_e^T and D_{ee} are the thermal and ordinary diffusion of electron, respectively.

$\left(D_e^T\right)_{add}$ and $(D_{ee})_{add}$ are thermal and ordinary diffusion coefficients respectively, which are induced by the ultrasound. ρ_e and ρ_h represent electron mass density and heavy particle mass density, respectively

According to [16], the total diffusion coefficients can be written as:

$$\left(D_e^T\right)_{us} = D_e^T + \theta_T \cdot \theta'_M \cdot \left(D_e^T\right)_{add} \tag{30}$$

$$(D_{ee})_{us} = D_{ee} + \theta_T \cdot \theta'_M \cdot (D_{ee})_{add} \tag{31}$$

$$\begin{aligned} \theta'_M = {} & \mathrm{b}_1 + \mathrm{b}_2 \cdot \log(n_1) + b_3 \cdot \log(n_2) + b_4 \cdot \log(n_1) \cdot \log(n_2) \\ & + b_5 \cdot [\log(n_1)]^2 + b_6 \cdot [\log(n_2)]^2 \end{aligned} \tag{32}$$

It can be found that both $\left(D_e^T\right)_{us}$ and $(D_{ee})_{us}$ consist of two terms. The first term is the diffusion coefficient when no ultrasound is applied (i.e.,$\nabla \cdot \vec{c}_0$ is equal to zero), and the second term is the additional diffusion coefficient due to the application of ultrasound. With application of ultrasound, the velocity gradient generated by ultrasound causes the change of particle density, thus affecting the diffusion coefficient. θ'_M is a correction coefficient related to particle concentration. Since electrons are significantly more affected by Ar^+ and Ar^{2+} than Ar, θ'_M is a function of ion concentration. Among them, the constants b_1, b_2, b_3, b_4, b_5, and b_6 can be obtained by using the method of obtaining a_1 and a_2.

3.2.4. (4) Electrical Conductivity Variation Induced by Ultrasound

Since the electrical conductivity is related to the ordinary diffusion coefficient, referring to Equation (31), we can get the formula to calculate the electrical conductivity when ultrasound is applied:

$$\sigma_{us} = -\frac{e^2 n_e n m_e}{\rho k_b T}(D_{ee})_{us} \tag{33}$$

3.2.5. (5) The term $\nabla\vec{C}_0$ related to velocity gradient of ultrasonic vibration

Equations (15), (16), (28), and (29) all include the term $\nabla \cdot \vec{c}_0$ which is related to the ultrasonic vibration velocity. In fact, it is the divergence of ultrasonic vibration velocity,

$$\nabla \cdot \vec{c}_0 = \frac{\partial v_z}{\partial z} + \frac{\partial v_r}{\partial r} \tag{34}$$

where v_z and v_r are the components of vibration velocity in z and r directions, respectively. Assuming that the vibration is emitted from the tip of the tungsten electrode, due to the phase difference between the vibrations at different positions [48], we have,

$$v = \frac{dS_0}{dt} = A_v \omega \cos(\omega\, t - k_0 L) \tag{35}$$

$$L = \sqrt{z^2 + r^2} \tag{36}$$

where S_0 is the displacement of the vibrating particle from the equilibrium position, $k_0 = \omega/c$, A_v is the amplitude, L is the distance between the vibrating position and the sound source. In order to simplify the calculation, we only consider the velocity gradient in the z direction, so we calculate the partial derivative of Equation (35):

$$\nabla \cdot \vec{c}_0 = \frac{\partial v_z}{\partial z} = \frac{z}{\sqrt{z^2 + r^2}} \frac{A_v \omega^2}{c} \sin\left[\omega\left(t - \frac{L}{c}\right)\right] \tag{37}$$

Equation (37) is a formula describing the velocity gradient at different positions in the sound field under ideal conditions, and the attenuation in the ultrasound propagation process is not considered in the formula. However, sound attenuation should be considered in the calculation process. Therefore, we need to replace Equation (37), instead of using $\frac{x}{\sqrt{z^2+r^2}} A_v$ to represent the amplitude of the corresponding position. We need to use the amplitude value obtained by numerical calculation introduced in Section 2.1. The calculated A_{v-cal} is different at different positions, so Equation (37) becomes

$$\nabla \cdot \vec{c}_0 = \frac{A_{v-cal} \omega^2}{c} \sin\left[\omega\left(t - \frac{\sqrt{z^2 + r^2}}{c}\right)\right]. \tag{38}$$

It can be found from Equation (26) that the velocity gradient tensor $\nabla \cdot \vec{c}_0$ is a function of time and coordinate position. That is, $\nabla \cdot \vec{c}_0$ varies at different times at different positions of the sound field. The value of $\nabla \cdot \vec{c}_0$ changes alternately in positive and negative directions. In a vibration period, when the vibration speed is positive or negative, the particles at the equilibrium position will deviate from their original positions by an amplitude A_v, which causes the interaction of particles at different positions. Therefore, when the ultrasonic vibration velocity is positive or negative, the effect of ultrasound on the transport coefficient is equivalent. Take a point with coordinate value (0,1). If the welding current is 80 A, the temperature at this point is 1.7569×10^4 K. The mean free path of heavy particles at this temperature calculated by Equation (7) is about 7.85×10^{-6} m, while the amplitude generated by ultrasound at this point is 1.68×10^{-5} m. The amplitude is about twice the mean free path. As schematically shown in Figure 4, assume the point (0,1) is O, the particles at O can move upward or

downward for two mean free paths to reach points Z_{up} and Z_{down}. Assume the temperature is the same in a mean free path, and the temperature at position O is T_0, the temperature of the first and the second mean free path at upper part referring to position O are T'_1 and T'_2, respectively. At the same time, the temperature of the first and the second mean free path at lower part referring to position O are T_1 and T_2, respectively, and $T'_2 > T'_1 > T_0 > T_1 > T_2$. When the particles vibrate downward to Z_{down} at the moment corresponding to one-quarter of the cycle ($T_{uv}/4$), the particles in the original three mean free paths are compressed into one mean free path, So the temperature at Z_{down} becomes the averaged temperature $(T_0 + T_1 + T_2)/3$. When the particles vibrate upward to O at the moment corresponding to half cycle ($T_{uv}/2$), the temperature at position O becomes the averaged temperature $(T_0 + T_1 + T_2)/3$. When the particles vibrate upward to Z_{up} at the moment corresponding to three-quarter of cycle ($3T_{uv}/4$), the temperature at Z_{up} becomes the averaged temperature $(T_1 + T_2)/3 + (T_0 + T_1 + T_2)/9$. Thereby, in a vibration period, the temperature at equilibrium position O has changed two times:

$$\text{The first time}: \ \Delta T_1 = \frac{T_0 + T_1 + T_2}{3} - T_0 \tag{39}$$

$$\text{The second time}: \ \Delta T_2 = \frac{T'_1 + T'_2}{3} - \frac{2(T_0 + T_1 + T_2)}{9} \tag{40}$$

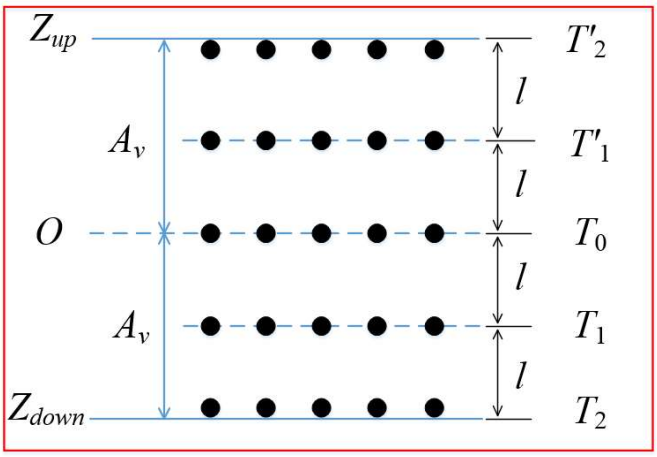

(**a**) 0

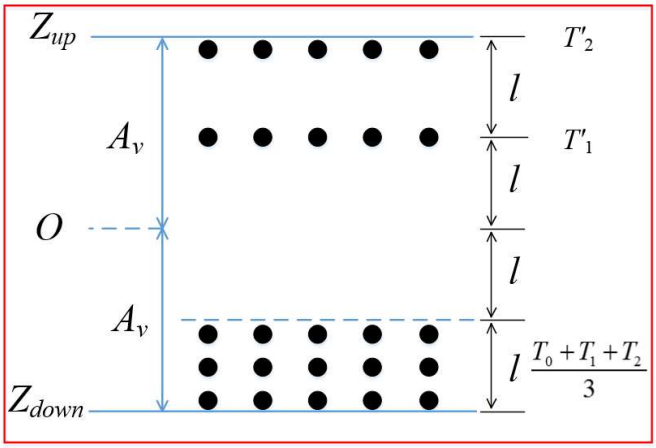

(**b**) $T_{us}/4$

Figure 4. *Cont.*

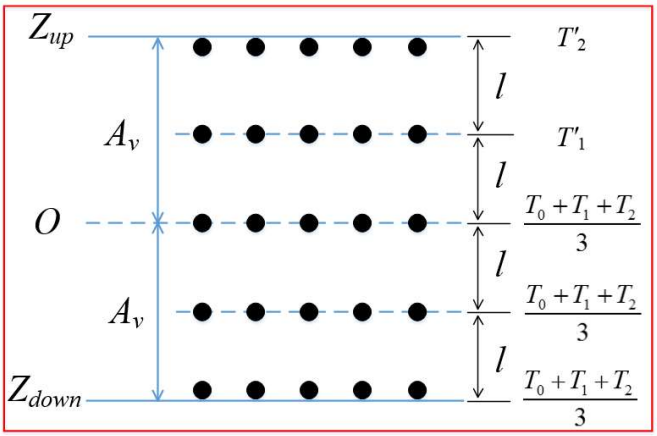

(**c**) $T_{\mathrm{us}}/2$

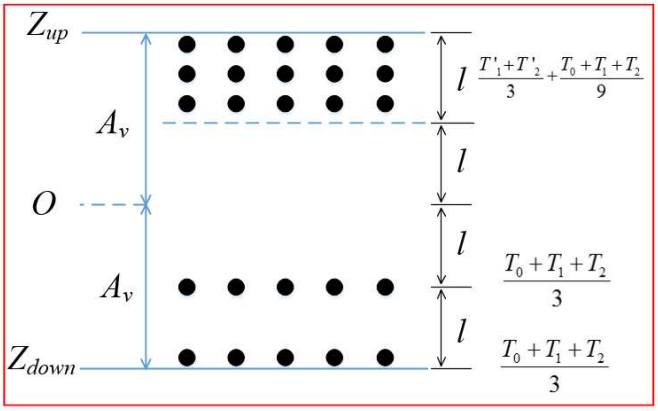

(**d**) $3T_{\mathrm{us}}/4$

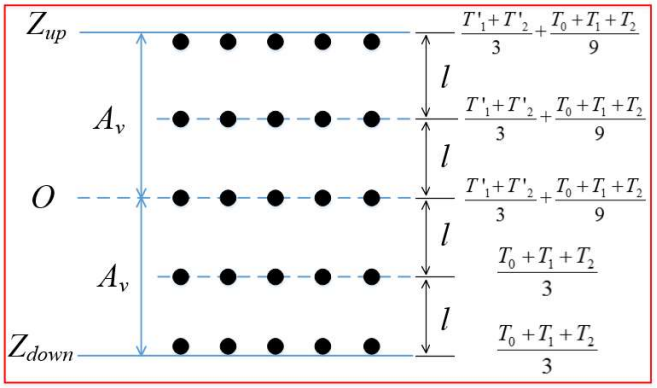

(**e**) T_{us}

Figure 4. Schematic of plasma gas temperature variation in one vibration period T_{us}.

It can be found that ultrasound produces a new heat transfer mode, resulting in an increase in thermal conductivity. It can be determined that whether the value of $\nabla \cdot \vec{c}_0$ is positive or negative, ultrasound always promotes heat conduction. Because $\nabla \cdot \vec{c}_0$ changes with time and conforms to the sine function, its effective value should be employed to describe the effects of ultrasonic vibration, i.e.,

$$\nabla \cdot \vec{c}_0 = \frac{\sqrt{2}}{2} \frac{A_{v-cal}\omega^2}{c} \tag{41}$$

where the amplitude A_{v-cal} of ultrasonic vibration is position dependent.

4. Solution Technique

In this study, the numerical simulation of plasma arc was realized by fluid dynamics software FLUENT 6.3 (Ansys, Inc. Canonsburg, PA, USA), and the simulation of ultrasonic propagation adopts the calculation results in Reference [13], and ultrasonic related data were coupled into PAW by using UDF (user-defined functions). The influence of ultrasound on the thermal and electrical conductivity of plasma is closely related to the sound pressure. Because the sound pressure in each position is different in U-PAW, the transport coefficients are not only the function of temperature, but also the function of sound pressure. In order to ensure the accuracy of the calculation of the transport coefficients, it is necessary to write the numerous analytical formulas of the transport coefficients into UDF through computer language, so as to ensure that when the transport coefficients are calculated on each grid, the sound pressure value on the corresponding grid node is called. At the same time, we also need to know the plasma composition of each grid cell, so we need to solve the equation group composed of the Saha equation, Dalton's law, and charge quasi-neutral condition. Because the equation group is a nonlinear multivariable equation group, FLUENT does not have the function of solving the equation group. We need to solve the equation group through Matlab (R2018a, The MathWorks, Inc. Natick, MA, USA) to obtain the plasma composition–temperature curve, and then write it into UDF as a function to calculate the transport coefficients. Segregated solver and PISO algorithm were chosen to solve control equations of plasma arc in FLUENT. This algorithm is takes pressure as the basic solution variable, has the function of adjacent correction, which is suitable for the calculation of transient model, and the calculation stability and convergence are better than SIMPLE algorithm.

5. Results and Discussion

The above-mentioned equations were employed to calculate the transport coefficients. The study cases are with following conditions: nozzle diameter is 3.2 mm, tungsten electrode setback is 2 mm, the distance between the nozzle exit and the anode surface is 5 mm, plasma gas flow rates is 2.8 L/min, and welding current is 100 A. The output power of the ultrasonic vibration system is 500 W, the amplitude is 20 μm, and frequency is 25 kHz.

By using Equation (16), the thermal conductivity of heavy particles when ultrasound is applied is calculated. Figure 5 compares the distribution of thermal conductivity of heavy particles in PAW and U-PAW. It can be seen that the thermal conductivity of heavy particles increases obviously if ultrasound is applied.

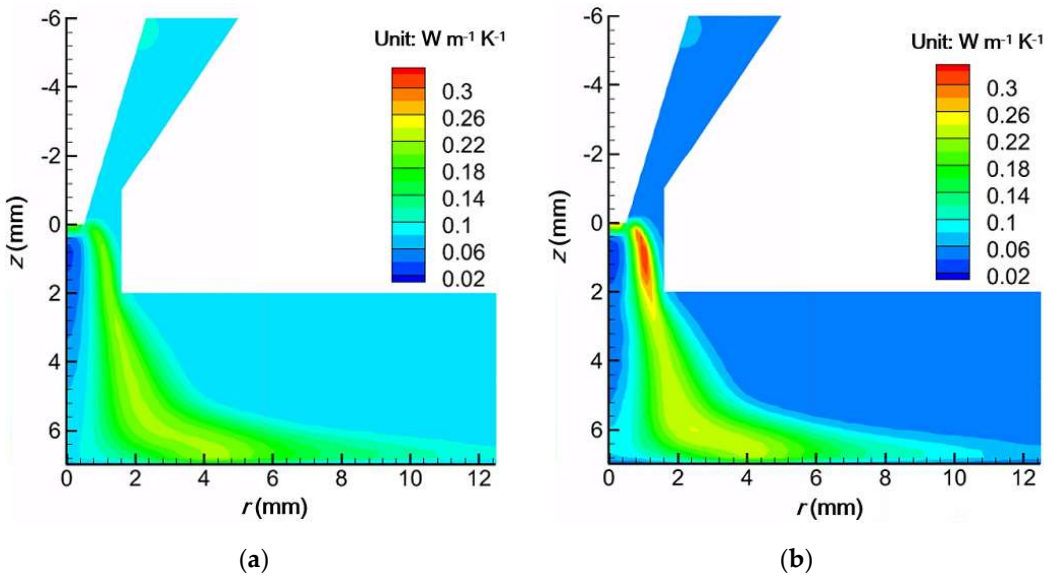

Figure 5. Distribution of thermal conductivity of heavy particles (**a**) PAW, (**b**) U-PAW.

A radial line with z-coordinate 0.5 mm is selected. This line is near the tungsten tip where ultrasonic vibration is strong. Along this line, the temperature drops as the radial distance increases so that whole temperature range is covered. The thermal conductivity of heavy particles versus temperature is drawn, as shown in Figure 6. This presents the comparison of calculated thermal conductivity of heavy particles with and without ultrasound. The thermal conductivity and viscosity of heavy particles without ultrasound are taken from [49,50]. When the temperature is around 6×10^3 K–1.4×10^4 K, the increase in thermal conductivity of heavy particles is obvious.

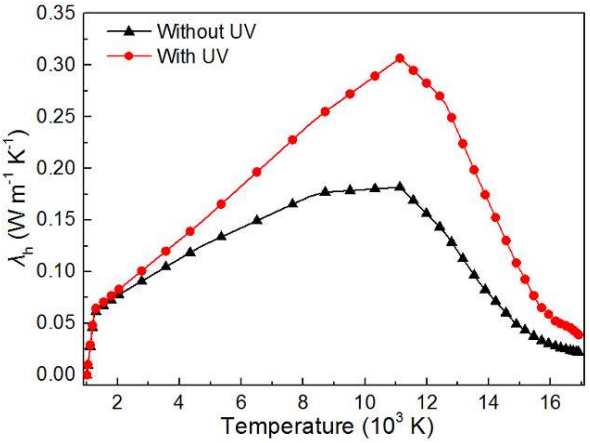

Figure 6. Thermal conductivity of heavy particles with/without ultrasonic vibration.

Figure 7 compares the distribution of electron thermal conductivity in PAW and U-PAW. Since ultrasound only has an effect on the second term in Equation (20), the difference between U-PAW and U-PAW is not obvious for the distribution of electron thermal conductivity. Figure 8 shows the changes of electron thermal conductivity in PAW and U-PAW at different temperature along the same line as aforementioned (z = 0.5 mm, r). It can be seen that the electron thermal conductivity increases a little bit after ultrasound is applied.

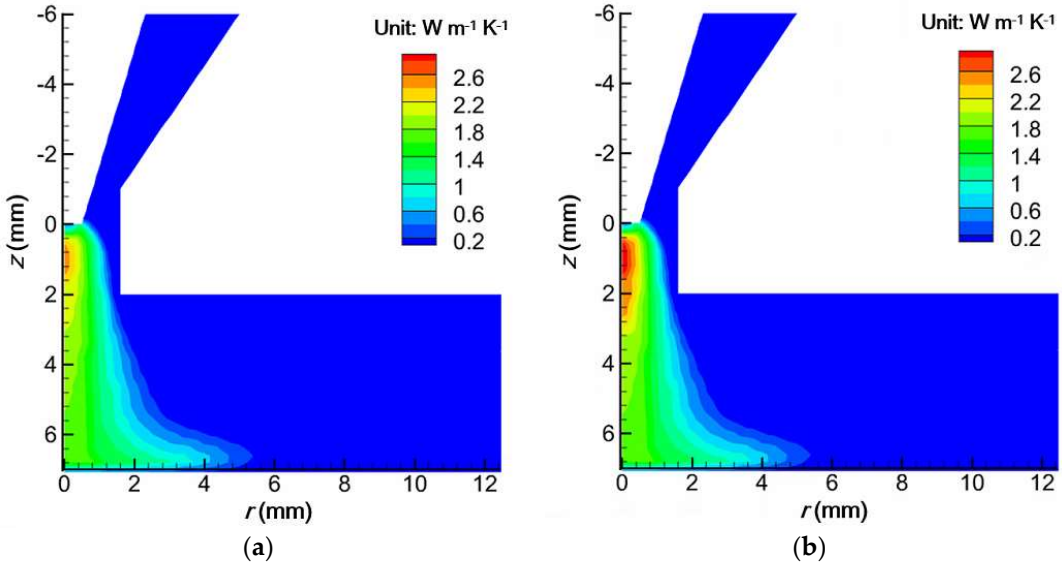

Figure 7. Distribution of electrons thermal conductivity (**a**) PAW, (**b**) U-PAW.

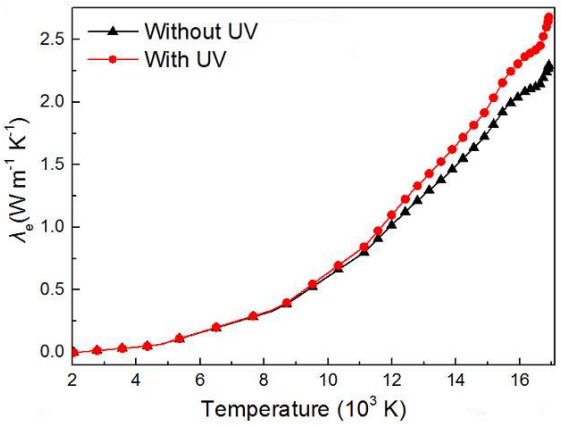

Figure 8. Electrons thermal conductivity with/without ultrasonic vibration.

Figures 9 and 10 compare the variations of the reaction thermal conductivity. Figure 10 shows the changes of reaction thermal conductivity in PAW and U-PAW at different temperature along the line (z = 0.5 mm, r). The reaction thermal conductivity obviously increases after ultrasound is applied.

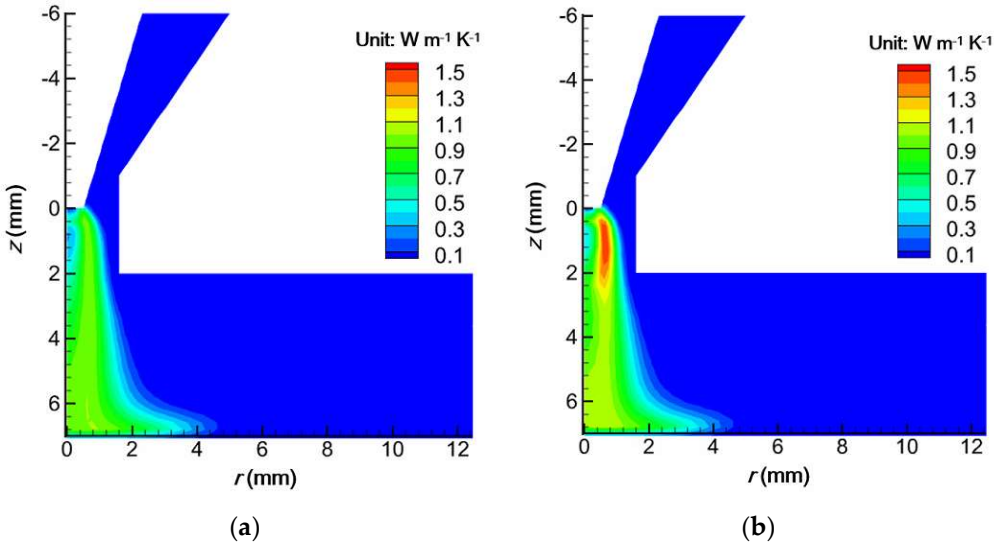

Figure 9. Distribution of reaction thermal conductivity (**a**) PAW, (**b**) U-PAW.

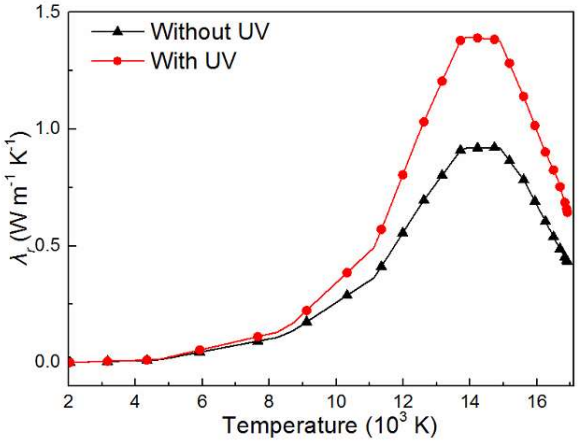

Figure 10. Reaction thermal conductivity with/without ultrasonic vibration along z = 0.5 mm.

Figure 11 shows the total thermal conductivity of plasma arc. It can be seen that when the temperature is higher than 1×10^4 K, the total thermal conductivity increases obviously, because the temperature near the tungsten electrode is higher and the amplitude of the ultrasound near the tungsten electrode is larger, so the thermal conductivity of plasma by ultrasound increases significantly. Another reason is that when the temperature is lower than 1×10^4 K, the ionization rate of argon plasma is lower and the electron concentration is smaller, so the increase of electron thermal conductivity by ultrasound is not obvious.

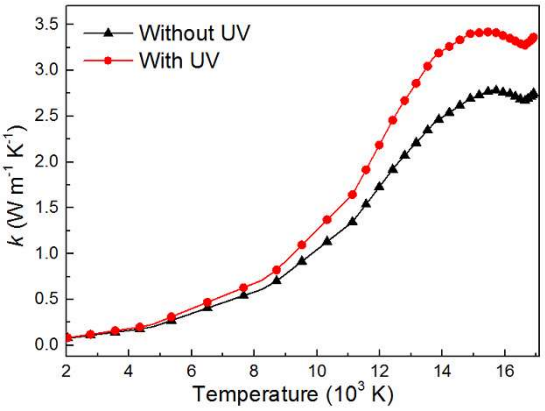

Figure 11. Total thermal conductivity of plasma arc with and without ultrasound.

Figure 12a illustrates a comparison of the thermal diffusion coefficient of plasma arc with and without ultrasound. The thermal diffusion coefficient is affected by the temperature gradient and the concentration gradient of each component. Because ultrasound causes a simultaneous increase in both temperature gradient and particle concentration within an amplitude range during the vibration process, the thermal diffusion coefficient D_e^T is increased when ultrasound is applied. However, as shown in Figure 12b, ultrasound makes the ordinary diffusion coefficient get a little bit lower. The reason is that the density of atoms and ions is not uniform because of the fluctuation of ultrasound. The dense regions of atoms and ions form a "wall" of heavy particles, which hinders the inter-diffusion of electrons on both sides of the "wall", resulting in the reduction of the ordinary diffusion coefficient D_{ee}.

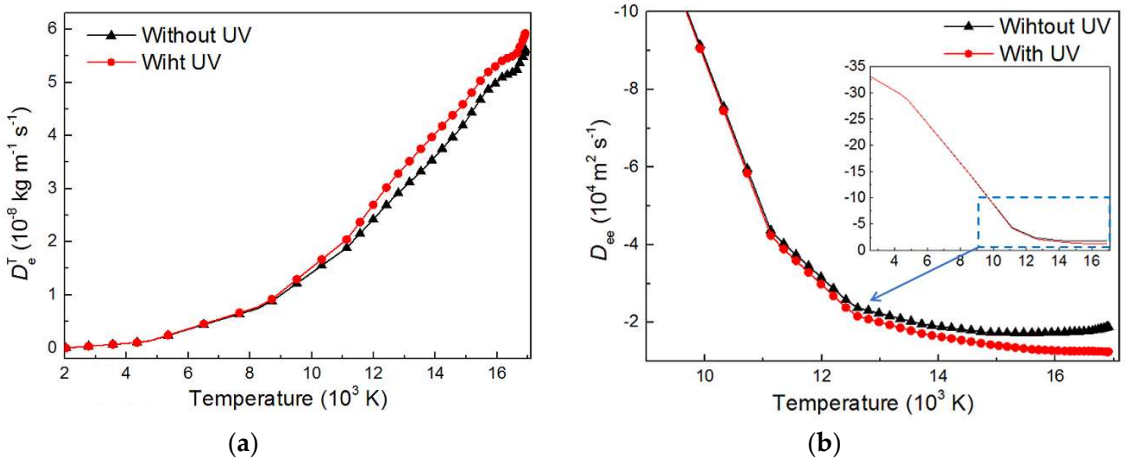

Figure 12. The diffusion coefficients with and without ultrasound. (**a**) Thermal diffusion coefficient, (**b**) Ordinary diffusion coefficient.

Figure 13 compares the distribution of electric conductivity in PAW and U-PAW. It is clear that the electric conductivity decreases after ultrasound is applied. Due to the high temperature in the center of the arc column, the electrical conductivity is also higher than the outside of the arc column,

as shown in Figure 14. At the same time, the ionization degree of argon atoms increases obviously at high temperature, so the effect of ultrasonic vibration on electrical conductivity will also increase. The reason is that when temperature is low, argon atoms are dominant in the plasma. Since argon atoms are neutral, their interaction with electrons is weak, so they do not have a great impact on the electrical conductivity. With the increase of temperature, the ionization degree of argon atoms increases, especially in the temperature range of 1×10^4 K–2×10^4 K, and a large amount of Ar^+ appears. Due to ultrasonic vibration, the density of Ar^+ alters between sparse and dense periodically. When Ar^+ is concentrated by ultrasound to form a high-density region, it will hinder the movement of electrons, resulting in a decrease in electrical conductivity. As the temperature continues to increase, Ar^{2+} in the plasma will reach a level that cannot be ignored. The large amount of Ar^{2+} under the action of ultrasound will further hinder the movement of electrons, thus causing a larger decrease of electrical conductivity.

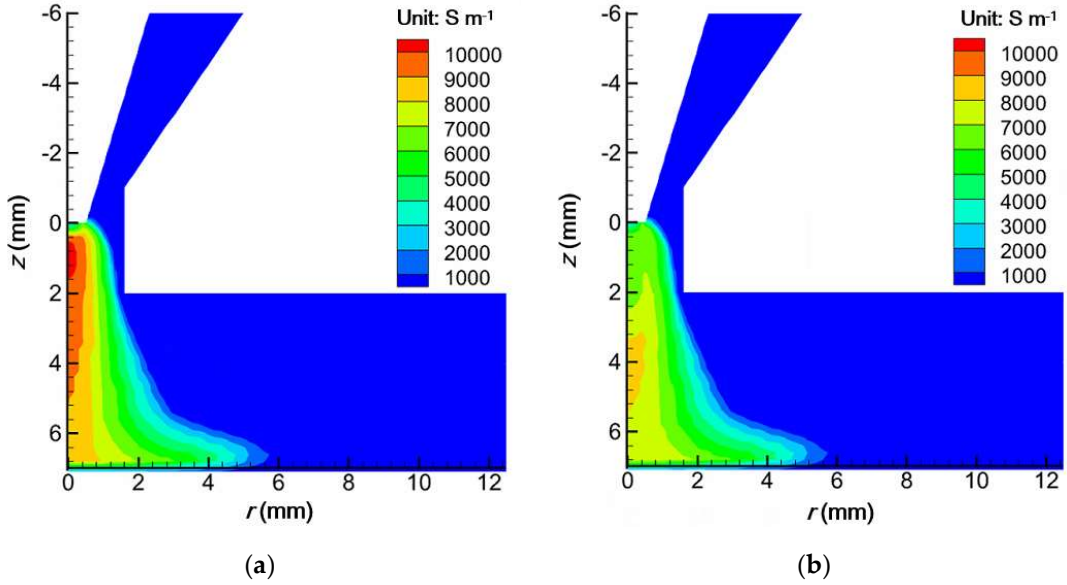

Figure 13. Distribution of Electrical conductivity (**a**) PAW, (**b**) U-PAW.

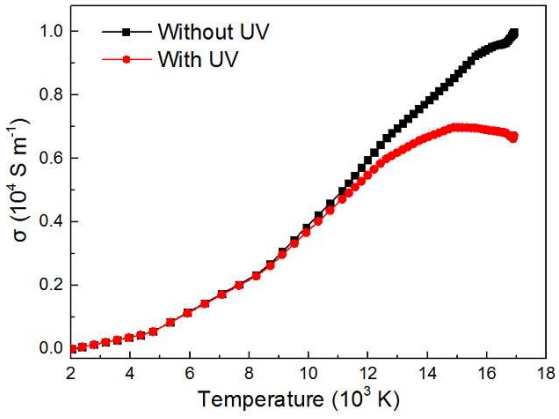

Figure 14. Comparison of electrical conductivity with and without ultrasound.

The calculated transport coefficients are employed to calculate the characteristics of plasma arc with and without ultrasonic vibration. Figures 15 and 16 compares the arc pressures at anode in PAW and U-PAW when the welding current is 100 A and the flow rate of plasma gas is 2.8 L/min. The stagnation pressure measurement apparatus was used to measure the pressure of the plasma arc [12]. The measuring device includes a water-cooled copper plate with a measuring hole of 0.5 mm

in diameter, a differential pressure sensor with a measuring range of 0–5 kPa and a data acquisition card. During the measurement process, the welding torch was fixed, and the water-cooled copper anode was controlled via a precise three-dimensional sliding platform, so the arc pressure at different positions of the plasma arc can be measured. At a specific position, measurement was carried out ten times, and the average value was obtained. It can be seen that the arc pressure in U-PAW is higher than that in PAW. In general, the predicted arc pressure is consistent with the measured value.

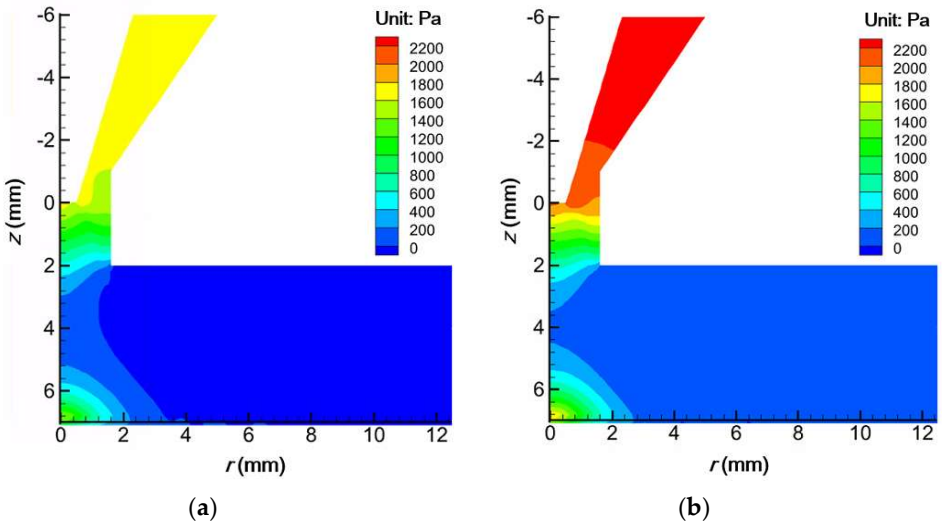

Figure 15. Distribution of arc pressure between (**a**) PAW and (**b**) U-PAW at 100 A.

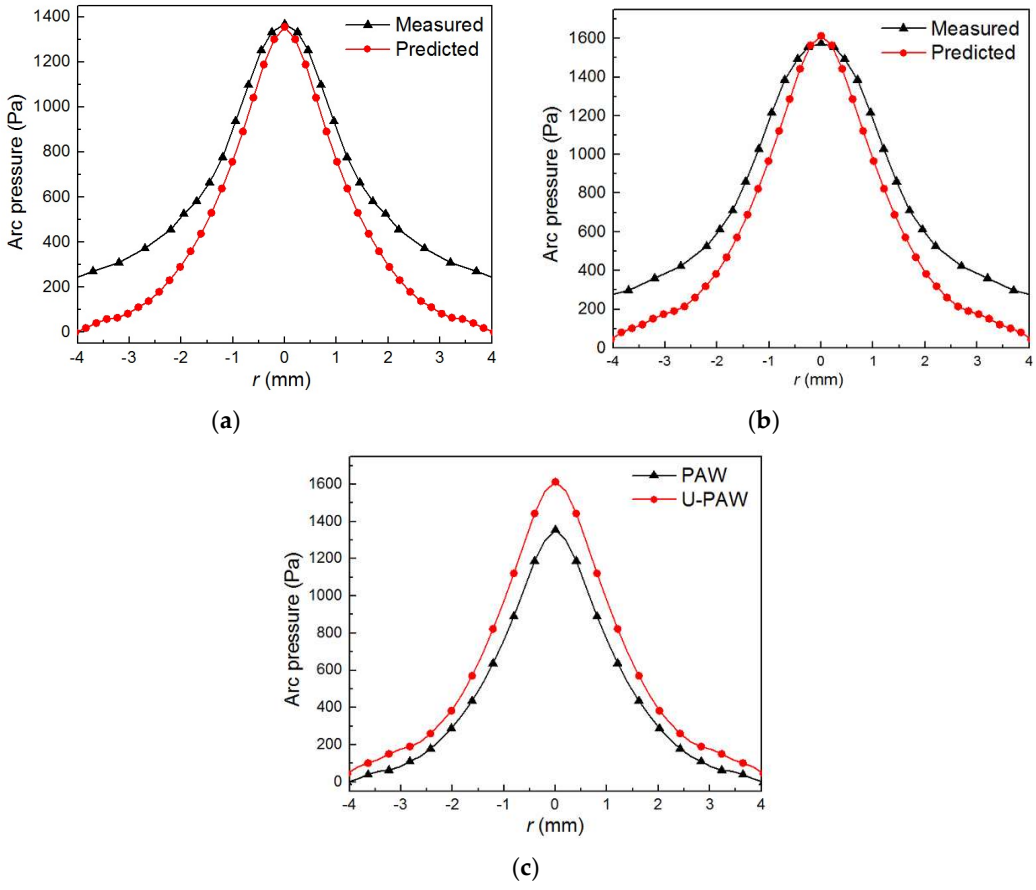

Figure 16. Comparison of arc pressure between (**a**) PAW; (**b**) U-PAW at 100 A; (**c**) Predicted arc pressure.

6. Conclusions

(1) The effective value of the ultrasound velocity gradient tensor is employed to describe the effects of ultrasonic vibration on transport coefficients in an ultrasound assisted plasma arc, and the calculation method of transport coefficients is developed.

(2) Ultrasound can increase the thermal conductivity of heavy particles. The ultrasonic vibration results in an increase of the electrons thermal conductivity and reaction thermal conductivity, but leads to a decrease of the electrical conductivity.

(3) Ultrasound increases the thermal diffusion coefficient D_e^T, and with the increase of temperature, the increment become more obvious. However, for the ordinary diffusion coefficient, due to the fluctuation of ultrasound, the density of atoms and ions is not uniform. The dense areas of atoms and ions form a "wall" of heavy particles, which hinders the inter-diffusion of electrons on both sides of the "wall", thus reducing the ordinary diffusion coefficient D_{ee}.

(4) The common and updated transport coefficients are applied to the model of plasma arc and the pressures of PAW and U-PAW on anode surface are predicted. The arc pressure of U-PAW is increased compared with that of PAW. The predicted values can be consistent with the measured ones.

Author Contributions: Y.L.: Investigation, Methodology, Numerical simulation, Validation, Writing—original draft. C.W.: Supervision, Investigation, Writing—review & editing. M.C.: Measurement. All authors have read and agreed to the published version of the manuscript.

Acknowledgments: The authors acknowledge the financial support from the National Natural Science Foundation of China (Grant No. 51775312).

Conflicts of Interest: The authors declare that they have no known competing financial interests or personal relationships that could have appeared to influence the work reported in this paper.

Nomenclature

A_v	Amplitude of ultrasound
A_{v-cal}	Calculated amplitude of ultrasound
a_{j1}	The first Sonine expansion coefficient of particle
a_{11}	The first Sonine expansion coefficient of electron
a_1,a_2	Adjustment coefficients of heavy particle thermal conductivity caused by ultrasound
$b_1 - b_6$	Adjustment coefficients of diffusion coefficient caused by ultrasound
c	Propagation velocity of ultrasound in plasma arc
$\vec{c}_0$	Vibration velocity of ultrasound
c_{ref}	Propagation velocity of ultrasound under normal temperature and pressure
$\vec{\vec{C}}$	Diffusion velocity
$\vec{C}$	Particle specific velocity relative to the plasma
$\vec{d}_{12}$	Diffusion driving force of binary gas
D^T	Thermal diffusion coefficient of binary gas
D_e^T	Thermal diffusion coefficient of electron
$\left(D_e^T\right)_{add}$	Additional thermal diffusion coefficient of electron because of ultrasound
$\left(D_e^T\right)_{us}$	Thermal diffusion coefficient of electron with ultrasound
$\left(D_i^T\right)_{us}$	Thermal diffusion coefficient of particle i with ultrasound
D_{12}	Ordinary diffusion coefficient of one component gas
D'_{12}	Ordinary diffusion coefficient of binary gas
D_{ee}	Ordinary diffusion coefficient of electron
$(D_{ee})_{add}$	Additional ordinary diffusion coefficient of electron because of ultrasound
$(D_{ee})_{us}$	Ordinary diffusion coefficient of electron with ultrasound
$\left(E_{ij}\right)_{us}$	An element of the inverse of a matrix whose general element is $\left(D_{ij}\right)_{us} m_j$

e	Electron charge
f	Velocity distribution function
$f^{(i)}$	The i-th approximation of velocity distribution function
f_v	Ultrasonic vibration frequency
$\overrightarrow{F}_j$	External force
$\overrightarrow{j}_e$	Conduction current density
h_p	Planck constant
$I_{T_1}^{(1)}$	The primary ionization rate of argon plasma at T_1
$I_{T_1}^{(2)}$	The secondary ionization rate of argon plasma at T_1
k	Total thermal conductivity
k_b	Boltzmann constant
l_e	Mean free path of electron
l_h	Mean free path of heavy particle
L	Distance between the vibrating position and the sound source
m_e	Mass of electron
m_h	Mass of heavy particle
m_j	Mass of particle j
n	Total particle concentration
n_0	Concentration of Ar
n_1	Concentration of Ar^+
n_2	Concentration of Ar^{2+}
n_e	Concentration of electron
n_h	Concentration of heavy particle
n_j	Concentration of particle j
n_{ref}	Reference concentration of heavy particles
p	Pressure
p_s	Acoustic pressure
p_0	Atmospheric pressure
p_{ms}	Acoustic pressure amplitude
p_{ref}	Reference acoustic pressure in gas
Q_e	Statistical weight of electron
Q_i	Partition function of particle i
$\overrightarrow{q}$	Thermal flux vector
$\overrightarrow{q}^{(1)}$	The first approximation thermal flux vector
$\overrightarrow{q}_{r-\mathrm{us}}$	Reaction thermal flux produced by ultrasonic vibration
$q_{ij}^{m_0 p_0}$	Bracket integrals
R	Gas constant
r	The component of cylindrical coordinate in r direction
S_0	Displacement of the vibrating particle from the equilibrium position
S	A small area to study reaction thermal flux
t	Time
T	Temperature
T_{ref}	Thermodynamic reference temperature
T_{us}	Period of ultrasonic vibration
u	Ultrasonic vibration velocity
u_m	Velocity amplitude of ultrasonic vibration
v_z	The component of vibration velocity in z direction
v_r	The component of vibration velocity in r direction
Z	Number of charges carried by Particles
z	The component of cylindrical coordinate in z direction

Greek symbols

γ_s	The acoustic pressure flux of boundary
ε_0	Vacuum dielectric constant
ε_i	The *i*-st ionization energy
$\Delta\varepsilon_i$	Decrease of ionization energy
λ_{h-us}	Thermal conductivity of heavy particles with ultrasound
λ_{us}	True electronic thermal conductivity with ultrasound
λ_{e-us}	True electronic thermal conductivity with ultrasound
λ_{r-us}	Reaction thermal conductivity caused by ultrasound
λ_D	Debye length
λ_r	Reaction thermal conductivity
μ	Viscosity
ρ	Gas density
ρ_e	Electron mass density
ρ_j	Mass density of particle j
ρ_h	Heavy particle mass density
σ	Electrical conductivity
σ_{us}	Electrical conductivity with ultrasound
σ_h	Heavy particle diameter
σ_e	Electron diameter
ω	Angular frequency of ultrasonic vibration

References

1. Wu, C.S.; Wang, L.; Ren, W.J.; Zhang, X.Y. Plasma arc welding-process, sensing, control and modeling. *J. Manuf. Process.* **2014**, *16*, 74–85. [CrossRef]
2. Gupta, M.R.; Reddy, M.R.; Mukherjee, M.M. Key-hole plasma arc welding of 8 mm thick maraging steel—A comparison with multi-pass GTAW. *Weld. World* **2012**, *56*, 69–75. [CrossRef]
3. Zhang, Y.M.; Zhang, S.B.; Jiang, M. Keyhole double-sided arc welding process. *Weld. J.* **2002**, *81*, 248s–255s.
4. Vredeveldt, H.L. Increased Power Density Plasma Arc Welding-the Effect of An Added Radial Gas Flow around the Arc Root. Ph.D. Thesis, Delft University of Technology, Delft, The Netherlands, 2014.
5. Wu, D.S.; Tashiro, S.; Wu, Z.A.; Nomura, K.; Hua, X.M.; Tanaka, M. Analysis of heat transfer and material flow in hybrid KPAW-GMAW process based on the novel three dimensional CFD simulation. *Int. J. Heat Mass Transf.* **2020**, *147*, 118921. [CrossRef]
6. Wang, B.; Zhu, X.M.; Zhang, H.C.; Zhang, H.T.; Feng, J.C. Characteristics of Welding and Arc Pressure in the Plasma–TIG Coupled Arc Welding Process. *Metals* **2018**, *8*, 512. [CrossRef]
7. Yao, P.; Zhou, K.; Huang, S.W. Process and Parameter Optimization of the Double-Pulsed GMAW Process. *Metals* **2019**, *9*, 1009. [CrossRef]
8. Wu, C.S.; Jia, C.B.; Chen, M.A. A Control system for keyhole plasma arc welding of stainless steel with medium thickness. *Weld. J.* **2010**, *89*, 225s–231s.
9. Liu, Z.M.; Liu, Y.K.; Wu, C.S.; Luo, Z. Control of keyhole exit position in plasma arc welding process. *Weld. J.* **2015**, *94*, 196s–202s.
10. Jiang, X.; Zhou, Y.J.; Shi, C.; Mao, D.H. Effects of Ultrasonic-Aided Quenching on the Corrosion Resistance of GB 35CrMoV Steel in Seawater Environment. *Metals* **2018**, *8*, 104. [CrossRef]
11. Zhang, Y.; Guo, Y.Q.; Chen, Y.; Kang, L.; Cao, Y.B.; Yang, S.P. Ultrasonic-Assisted Laser Metal Deposition of the Al 4047Alloy. *Metals* **2019**, *9*, 1111. [CrossRef]
12. Wu, C.S.; Zhao, C.Y.; Zhang, C.; Li, Y.F. Ultrasonic vibration assisted keyholing plasma arc welding. *Weld. J.* **2017**, *96*, 279s–286s.
13. Li, Y.F.; Wu, C.S.; Chen, M.A. Numerical analysis of the ultrasound induced arc pressure increment in plasma arc welding. *J. Phys. D Appl. Phys.* **2019**, *52*, 035201. [CrossRef]
14. Ferziger, J.H.; Kaper, H.G. *Mathematical Theory of Transport Processes in Gases*; North-Holland Publishing Company, Ltd.: London, UK, 1972; pp. 9–298.
15. Chapman, S.; Cowling, T.G. *The Mathematical Theory of Non-Uniform Gases (Chinese Version)*; Cambridge University Press: Cambridge, UK, 1970; pp. 12–390.

16. Hirschfelder, J.O.; Curtiss, C.F.; Bird, R.B. *Molecular Theory of Gases and Liquids*; Wiley: New York, NY, USA, 1954; pp. 441–659.
17. Guo, X.X.; Murphy, A.B.; Li, X.W. Thermodynamic properties and transport coefficients of two-temperature helium thermal plasmas. *J. Phys. D Appl. Phys.* **2017**, *50*, 125202. [CrossRef]
18. Niu, C.P.; Chen, Z.X.; Rong, M.Z.; Wang, C.L.; Wu, Y.; Yang, F.; Wang, X.H.; Pang, Q.P. Calculation of 2-temperature plasma thermo-physical properties considering condensed phases: Application to CO_2–CH_4 plasma: Part 2. Transport coefficients. *J. Phys. D Appl. Phys.* **2016**, *49*, 405204. [CrossRef]
19. Guo, X.X.; Li, X.W.; Murphy, A.B.; Zhao, H. Calculation of thermodynamic properties and transport coefficients of CO_2–O_2–Cu mixtures. *J. Phys. D Appl. Phys.* **2017**, *50*, 345203. [CrossRef]
20. Yang, A.J.; Liu, Y.; Sun, B.W.; Wang, X.H.; Cressault, Y.; Zhong, L.L.; Rong, M.Z.; Wu, Y.; Niu, C.P. Thermodynamic properties and transport coefficients of high-temperature CO_2 thermal plasmas mixed with C_2F_4. *J. Phys. D Appl. Phys.* **2015**, *48*, 495202. [CrossRef]
21. Murphy, A.B.; Tanaka, M.; Yamamoto, K.; Tashiro, S.; Sato, T.; Lowke, J.J. Modelling of thermal plasmas for arc welding: The role of the shielding gas properties and of metal vapour. *J. Phys. D Appl. Phys.* **2009**, *42*, 194006. [CrossRef]
22. Park, H.; Trautmann, M.; Tanaka, K.; Tanaka, M.; Murphy, A.B. A computational model of gas tungsten arc welding of stainless steel: The importance of considering the different metal vapours simultaneously. *J. Phys. D Appl. Phys.* **2018**, *51*, 395202. [CrossRef]
23. Tanaka, K.; Shigeta, M.; Tanaka, M.; Murphy, A.B. Investigation of the bilayer region of metal vapor in a helium tungsten inert gas arc plasma on stainless steel by imaging spectroscopy. *J. Phys. D Appl. Phys.* **2019**, *52*, 354003. [CrossRef]
24. Park, H.; Trautmann, M.; Tanaka, K.; Tanaka, M.; Murphy, A.B. Mixing of multiple metal vapours into an arc plasma in gas tungsten arc welding of stainless steel. *J. Phys. D Appl. Phys.* **2017**, *50*, 43LT03. [CrossRef]
25. Wu, D.S.; Tashiro, S.; Hua, X.M.; Tanaka, M. Analysis of the energy propagation in the keyhole plasma arc welding using a novel fully coupled plasma arc-keyhole-weld pool model. *Int. J. Heat Mass Transf.* **2019**, *141*, 604–614. [CrossRef]
26. Jian, X.X.; Wu, C.S. Numerical analysis of the coupled arc–weld pool–keyhole behaviors in stationary plasma arc welding. *Int. J. Heat Mass Transf.* **2015**, *84*, 839–847. [CrossRef]
27. Chen, X.; Mu, Z.Y.; Hu, R.Z.; Liang, L.J.; Murphy, A.B.; Pang, S.Y. A unified model for coupling mesoscopic dynamics of keyhole, metal vapor, arc plasma, and weld pool in laser-arc hybrid welding. *J. Manuf. Process.* **2019**, *41*, 119–134. [CrossRef]
28. Xu, B.; Tashiro, S.; Jiang, F.; Tanaka, M.; Chen, S.J. The effect of electrode energy balance on variable polarity plasma arc pressure. *Int. J. Heat Mass Transf.* **2019**, *145*, 118715. [CrossRef]
29. Wu, D.S.; Nguyen, A.V.; Tashiro, S.; Hua, X.M.; Tanaka, M. Elucidation of the weld pool convection and keyhole formation mechanism in the keyhole plasma arc welding. *Int. J. Heat Mass Transf.* **2019**, *131*, 920–931. [CrossRef]
30. Bai, X.W.; Colegrove, P.; Ding, J.L.; Zhou, X.M.; Diao, C.L.; Bridgeman, P.; Hönnige, J.R.; Zhang, H.O.; Williams, S. Numerical analysis of heat transfer and fluid flow in multilayer deposition of PAW-based wire and arc additive manufacturing. *Int. J. Heat Mass Transf.* **2018**, *124*, 504–516. [CrossRef]
31. Feng, N. *Ultrasonics Handbook*; Nanjing University Press: Nanjing, China, 1999; pp. 48–59.
32. Ding, H. *Computational Ultrasonics–Analysis and Application of Ultrasonic Field*; Science Press: Beijing, China, 2010; pp. 10–11.
33. Shi, L. Numerical Analysis of Thermal Processes and Plastic Material Flow in Ultrasonic Vibration Enhenced Friction Stir Welding. Ph.D. Thesis, Shandong University, Shandong, China, 2016.
34. Trelles, J.P.; Heberlein, J.V.R.; Pfender, E. Non-equilibrium modelling of arc plasma torches. *J. Phys. D Appl. Phys.* **2007**, *40*, 5937. [CrossRef]
35. Chen, X.; Han, P. On the thermodynamic derivation of the Saha equation modified to a two-temperature plasma. *J. Phys. D Appl. Phys.* **1999**, *32*, 1711–1718. [CrossRef]
36. Colombo, V.; Ghedini, E.; Sanibondi, P. Two-temperature thermodynamic and transport properties of argon–hydrogen and nitrogen–hydrogen plasmas. *J. Phys. D Appl. Phys.* **2009**, *42*, 055213. [CrossRef]
37. Chen, D.M.; Hsu, K.C.; Pfender, E. Two-temperature modelling of an arc plasma reactor. *Plasma Chem. Plasma Process.* **1981**, *1*, 295–314. [CrossRef]

38. Murphy, A.B. Transport coefficients of hydrogen and argon–hydrogen plasmas. *Plasma Chem. Plasma Process.* **2000**, *20*, 279–297. [CrossRef]
39. Murphy, A.B.; Tam, E. Thermodynamic properties and transport coefficients of arc lamp plasmas: Argon, krypton and xenon. *J. Phys. D Appl. Phys.* **2014**, *47*, 295202. [CrossRef]
40. Murphy, A.B. Transport coefficients of plasmas in mixtures of nitrogen and hydrogen. *Chem. Phys.* **2012**, *398*, 64–72. [CrossRef]
41. Murphy, A.B. Transport coefficients of helium and argon–helium plasmas. *IEEE Trans. Plasma Sci.* **1997**, *25*, 809–814. [CrossRef]
42. Murphy, A.B.; Arundell, C.J. Transport coefficients of argon, nitrogen, oxygen, argon-nitrogen, and argon-oxygen plasmas. *Plasma Chem. Plasma Process.* **1994**, *14*, 452–490. [CrossRef]
43. Colombo, V.; Ghedini, E.; Sanibondi, P. Thermodynamic and transport properties in non-equilibrium argon, oxygen and nitrogen thermal plasmas. *Prog. Nucl. Energy* **2008**, *50*, 921–933. [CrossRef]
44. Zhang, X.N. The Study of the Transport Properties for Non-Equilibrium Thermal Plasmas. Ph.D. Thesis, University of Science and Technology of China, Anhui, China, 2015.
45. Devoto, R.S. The Transport Properties of a Partially Ionized Monatomic Gas. Ph.D. Thesis, Stanford University, San Francisco, CA, USA, 1965.
46. Devoto, R.S. Transport Properties of Ionized Monatomic Gases. *Phys. Fluids* **1966**, *9*, 1230–1240. [CrossRef]
47. Chapman, S.; Cowling, T.S. The velocity of diffusion in a mixed gas: The second approximation. *Proc. R. Soc. A* **1941**, *179*, 159–169.
48. Zhao, W.Z.; Wu, C.S. Constitutive equation including acoustic stress work and plastic strain for modeling ultrasonic vibration assisted friction stir welding process. *Int. J. Mach Tool Manuf.* **2019**, *145*, 103434. [CrossRef]
49. Zhang, X.N.; Li, H.P.; Murphy, A.B.; Xia, W.D. Comparison of the transport properties of two-temperature argon plasmas calculated using different methods. *Plasma Sources Sci. Technol.* **2015**, *24*, 035011. [CrossRef]
50. Capitelli, M.; Colonna, G.; Gorse, C.; D'Angola, A. Transport properties of high temperature air in local thermodynamic equilibrium. *Eur. Phys. J. D* **2000**, *11*, 279–289. [CrossRef]



© 2020 by the authors. Licensee MDPI, Basel, Switzerland. This article is an open access article distributed under the terms and conditions of the Creative Commons Attribution (CC BY) license (http://creativecommons.org/licenses/by/4.0/).